Satellite-Based Precipitation Estimation and Its Application for Streamflow Prediction over Mountainous Western U.S. Basins

ALI BEHRANGI, KONSTANTINOS ANDREADIS, JOSHUA B. FISHER, F. JOSEPH TURK, STEPHANIE GRANGER, THOMAS PAINTER, AND NARENDRA DAS

Jet Propulsion Laboratory, California Institute of Technology, Pasadena, California

(Manuscript received 6 March 2014, in final form 28 June 2014)

ABSTRACT

Recognizing the importance and challenges inherent to the remote sensing of precipitation in mountainous areas, this study investigates the performance of the commonly used satellite-based high-resolution precipitation products (HRPPs) over several basins in the mountainous western United States. Five HRPPs [Tropical Rainfall Measuring Mission 3B42 and 3B42-RT algorithms, the Climate Prediction Center morphing technique (CMORPH), Precipitation Estimation from Remotely Sensed Imagery Using Artificial Neural Networks (PERSIANN), and the PERSIANN Cloud Classification System (PERSIANN-CCS)] are analyzed in the present work using ground gauge, gauge-adjusted radar, and *CloudSat* precipitation products. Using ground observation of precipitation and streamflow, the skill of HRPPs and the resulting streamflow simulations from the Variable Infiltration Capacity hydrological model are cross-compared. HRPPs often capture major precipitation events but seldom capture the observed magnitude of precipitation over the studied region and period (2003–09). Bias adjustment is found to be effective in enhancing the HRPPs and resulting streamflow simulations. However, if not bias adjusted using gauges, errors are typically large as in the lower-level precipitation inputs to HRPPs. The results using collocated Advanced Microwave Scanning Radiometer for Earth Observing System (AMSR-E) and *CloudSat* precipitation data show that missing data, often over frozen land, and limitations in retrieving precipitation from systems that lack frozen hydrometeors contribute to the observed microwave-based precipitation errors transferred to HRPPs. Over frozen land, precipitation retrievals from infrared sensors and microwave sounders show some skill in capturing the observed precipitation climatology maps. However, infrared techniques often show poor detection skill, and microwave sounding in dry atmosphere remains challenging. By recognizing the sources of precipitation error and in light of the operation of the Global Precipitation Measurement mission, further opportunity for enhancing the current status of precipitation retrievals and the hydrology of cold and mountainous regions becomes available.

1. Introduction

Precipitation is a critical input for hydrologic simulation and prediction, and is widely used for agriculture, water resources management, and prediction of flood and drought, among other activities (Wu et al. 2012; Hong et al. 2007; Kucera et al. 2013). Precipitation is commonly measured by ground-based instruments (e.g., radar or rain gauge), but such instruments are sparse in time and space or nonexistent, even in many populated regions. With the global decline of in situ networks for hydrologic measurements (Stokstad 1999; Shiklomanov et al. 2002) and the growing demands for higher spatiotemporal resolution, remote sensing of precipitation is becoming a critical component of hydrometeorological research and applications. Recognizing challenges in accurate estimation of precipitation and the need for higher spatiotemporal resolution of precipitation products, efforts are under way to improve remote sensing observations and retrieval techniques. For example, the upcoming Global Precipitation Measurement (GPM) mission (Hou et al. 2013) will serve as an advanced standard for remote sensing of precipitation and will provide more accurate and consistent observations using a network of existing satellites united by the GPM core platform.

Three major types of spaceborne sensors are used for precipitation estimation: infrared (IR), passive microwave

Corresponding author address: Ali Behrangi, Jet Propulsion Laboratory, California Institute of Technology, 4800 Oak Grove Dr., MS 233-304, Pasadena, CA 91109.
E-mail: ali.behrangi@jpl.nasa.gov

DOI: 10.1175/JAMC-D-14-0056.1

(MW), and radar. The main advantage of IR-based precipitation retrieval is the availability of IR data at high spatiotemporal resolution [e.g., $\sim(0.04° \times 0.04°)$ grid every 30 min or less] from geostationary platforms, such as the Geostationary Operational Environmental Satellite. While combinations of visible and several IR channels have been found to be more effective (e.g., Behrangi et al. 2009, 2010) than a single IR channel, such observations mainly provide information about cloud top but shed little light on hydrometeors within clouds. MW sensors are commonly used to retrieve instantaneous precipitation estimates over land and ocean (e.g., Kummerow et al. 2011; Ferraro et al. 2005) with their estimates usually being more accurate than IR-based estimates, especially over ocean (Behrangi et al. 2012). Moreover, MW sensors can capture hydrometeor signals from the entire atmosphere using a combination of low- and high-frequency channels. However, over land, the radiometrically large surface emission and the variety of complex terrain hamper the ability to distinguish rain from the background (Ferraro et al. 1994; Ferraro et al. 2013). So far, MW retrieval techniques rely mainly on indirect-scattering-based schemes over land (Wilheit et al. 2003; Ferraro et al. 2005; Gopalan et al. 2010) to mitigate the surface contamination of signals. Therefore, MW-based precipitation estimates can miss precipitation events over land, especially warm rainfall that lacks ice particles. Furthermore, distinguishing between light rain and clouds from MW channels is often difficult (Berg et al. 2006; Lebsock and L'Ecuyer 2011), producing additional sources of uncertainty over land and ocean. More accurate precipitation estimates can be obtained from radars, providing vertical reflectivity of hydrometeors. Current space radars [e.g., precipitation radar on the Tropical Rainfall Measuring Mission (TRMM) and cloud profiling radar on *CloudSat*] have relatively long revisit times and narrow scan swaths, limiting their direct use in the generation of satellite combined high-resolution precipitation products (HRPPs). An additional source of useful precipitation data, particularly in higher latitudes and winter seasons, are short-term forecasts from numerical weather prediction models (Kidd et al. 2013; Zhang et al. 2013). However, to focus the purpose of this study, we restrict the analysis to well-established HRPPs.

Motivated by the growing demand for higher spatiotemporal precipitation datasets, HRPPs are produced by combining high spatiotemporal resolution but lower-accuracy IR images with more accurate but lower spatiotemporal resolution MW precipitation estimates using various methods (Huffman et al. 2007; Joyce et al. 2004; Behrangi et al. 2010; Kuligowski 2002; Hsu et al. 1997; Turk and Miller 2005). The skill of such products can vary substantially both regionally and seasonally, depending on the combination technique. Therefore, several studies have evaluated the performance of such products and have quantified the errors (Tian et al. 2007; Tian and Peters-Lidard 2010; Dinku et al. 2010; Kidd et al. 2012). HRPPs have also been compared with respect to their performance for hydrologic prediction whereby HRPPs are used to force hydrologic models to simulate streamflow, which is then compared with the observed streamflow (e.g., Hong et al. 2007; Hossain and Anagnostou 2004; Yilmaz et al. 2005; Behrangi et al. 2011; Gebregiorgis et al. 2012). Such analyses are important for identifying regional and seasonal strengths and weaknesses of the products, guiding users, and providing feedback to algorithm developers. However, only a limited number of studies have focused on assessing the efficacy of HRPPs over cold and mountainous regions and their hydrologic impacts. These regions are especially important for freshwater supply and management in the United States and many areas around the world. Krakauer et al. (2013) evaluated several HRPPs and station-based gridded precipitation products against weather station precipitation observations over Nepal and found that, if not bias adjusted using gauges, HRPPs significantly underestimate monthly precipitation volumes. Furthermore, they showed that none of the HRPPs fully captured the elevation dependence of mean precipitation. Bitew et al. (2012) show that TRMM 3B42-RT algorithm and Climate Prediction Center morphing technique (CMORPH) products perform better than the TRMM 3B42 and Precipitation Estimation from Remotely Sensed Imagery Using Artificial Neural Networks (PERSIANN) products in an Ethiopian mountain basin, which differs from the results found by several other studies (e.g., Tobin and Bennett 2010; Behrangi et al. 2011; Krakauer et al. 2013) as TRMM 3B42-RT and CMORPH are not bias adjusted by ground instruments. They found that when compared with rain gauge data, significant improvements in streamflow simulations are obtained when the model is calibrated with input-specific rainfall data. Focusing on heavy precipitation events, Stampoulis et al. (2013) used CMORPH and PERSIANN and high-quality weather radar rainfall estimates as a reference to study seven major flood-inducing events that developed over complex terrain areas in northern Italy and southern France. They found that while estimation errors are larger in convective-type precipitation, a majority of low rain rates in stratiform-type systems can be missed by the two studies precipitation products. Overall, studies suggest that the performance of the HRPPs vary greatly worldwide and it is not feasible to identify a single product performing the best everywhere.

Of particular importance to this study, mountainous regions often experience snowfall, frozen ground, and orographically induced precipitation that complicate the retrieval of precipitation from remote sensing. This study assesses the efficacy of several HRPPs in the San Joaquin–Sacramento basins of the Sierra Nevada range in California, which provide water for some of the richest farmlands in the United States and the world, and is a critical source of drinking water. Most of the annual precipitation in this region falls during the winter season in the form of extreme rain or snowfall, often brought by atmospheric rivers (Neiman et al. 2008; Dettinger 2011; Guan et al. 2010). Atmospheric rivers often cause the most intense precipitation storms in California, resulting in severe floods (Baird and Robles 1997; Ralph and Dettinger 2011).

The purpose of this manuscript is to investigate 1) how satellite precipitation products perform over a number of representative subbasins in the study region that experience a diverse range of snowfall-to-total precipitation ratios, 2) how the observed differences in the HRPPs impact the simulation of streamflow, and 3) what causes discrepancies between ground and satellite estimates of precipitation. The analysis of the streamflow also provides a secondary check for assessing the precipitation products through comparison with streamflow observations at the basin outlets. By extension, the outcome of this study can shed light on the performance and the level of maturity of HRPPs for hydrometeorological applications in mountainous basins, where ground observations of precipitation are sparse or nonexistent. This effort builds upon the longstanding precipitation validation program of the International Precipitation Working Group (IPWG; Ebert et al. 2007). The IPWG has the role of leadership for the Group on Earth Observations precipitation subtask (Kucera and Lapeta 2013). It also sets the stage for the implementation of newly designed HRPPs products that will be available in the GPM era such as the Integrated Multisatellite Retrievals for GPM (IMERG; Huffman et al. 2013).

2. Study area, hydrologic model, and datasets

Geographical locations of 22 studied subbasins in the San Joaquin–Sacramento, California, region, are shown in Fig. 1 with the topography map in the background. The basins were selected based on the size (>1000 km^2) and availability of uninterrupted streamflow observations at their outlets; these basins eventually drain into the Sacramento and San Joaquin valleys. The basins span a range of elevations (from ~150 to ~3000 m above sea level) and ratios of annual snowfall to total precipitation (from 0% to more than 40%). The Variable Infiltration Capacity (VIC) hydrological model (Liang et al. 1996; Liang and Xie 2001) was used to simulate streamflow at daily time scales. The model is a widely used semidistributed hydrologic model that has been successfully applied over numerous areas (e.g., Nijssen et al. 2001; Andreadis et al. 2005). VIC solves a water energy and mass balance over a rectangular grid, and accounts for a number of hydrologic processes (e.g., cold land processes, lakes, wetlands), resulting in a fairly comprehensive large-scale land surface model. Streamflow is simulated by routing the generated surface runoff and baseflow from each model grid cell, using a simple linear transfer function (Lohmann et al. 1998). VIC-simulated streamflow has been extensively validated, matching observations quite well (Maurer et al. 2002).

VIC requires a set of meteorological forcings, as well as information on the basin topography, land cover, and soils. The minimum forcing requirements for VIC include daily precipitation, maximum and minimum air temperature, and wind speed. Topography for the Sacramento–San Joaquin basins is derived from the 1-km Digital Elevation Model of the Global 30 arc s elevation dataset (GTOPO30), while a land cover map is obtained from Advanced Very High Resolution Radiometer imagery (Defries et al. 2000). Soil characteristics are the same as the ones used in Maurer et al. (2002), which were derived from a 1-km dataset (Miller and White 1998). Calibration of the model is performed by usually varying soil parameters such as hydraulic conductivity, with the parameters used for the simulations in this study obtained from the North American Land Data Assimilation System (NLDAS) experiment (Lohmann et al. 2004).

Simulations are performed over the study area for the period between 1 January 2000 and 31 December 2009 with the first 3 yr being used as a spinup period. VIC simulates hydrologic states and fluxes daily at a spatial resolution of 1/16° (~6 km).

a. Precipitation

1) SATELLITE PRODUCTS

The HRPPs utilized in the present study are 1) TRMM 3B42 real-time, version 7 (T3B42-RT; Huffman et al. 2007; Huffman and Bolvin 2014), 2) TRMM 3B42 research product, version 7 (T3B42; Huffman et al. 2007; Huffman and Bolvin 2014), 3) CMORPH (Joyce et al. 2004), 4) PERSIANN (Hsu et al. 1997; Sorooshian et al. 2000), and 5) the PERSIANN Cloud Classification System (PERSIANN-CCS, hereinafter referred to as CCS; Hong et al. 2004).

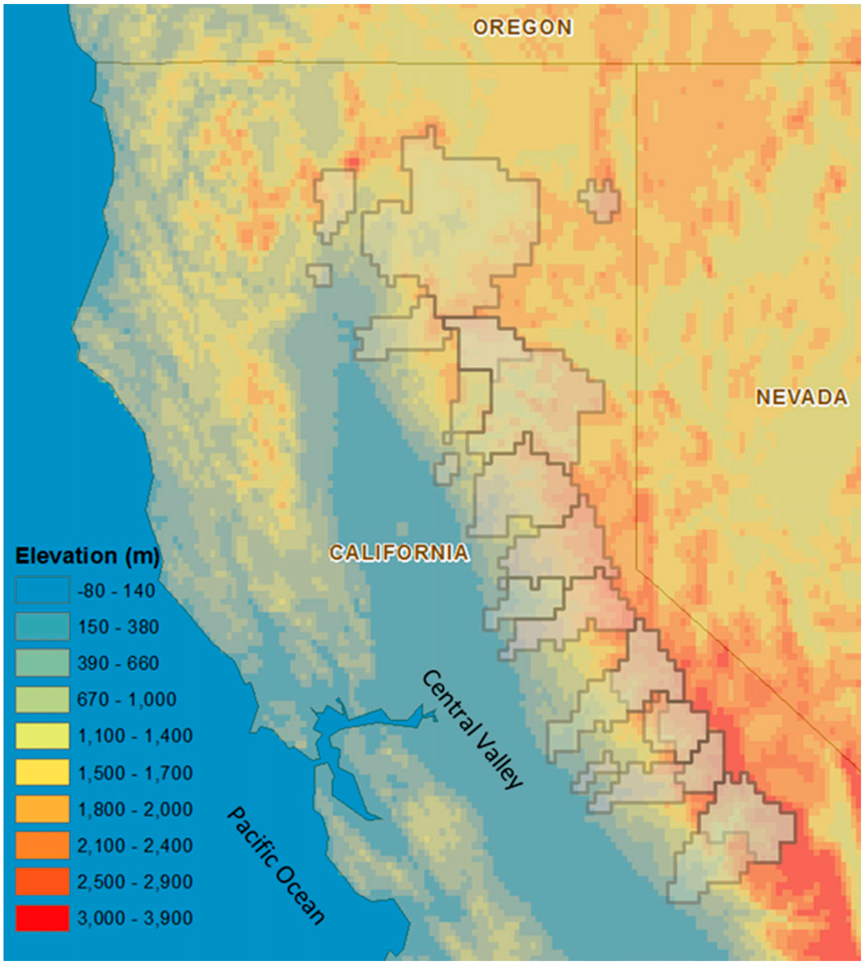

FIG. 1. Geographical location of the 22 studied basins shown with underlying topography.

T3B42-RT collects available MW-derived precipitation estimates from various MW sensors within a time bracket of 3 h, maps the MW precipitation data onto $0.25° \times 0.25°$ grids, and fills the remained gaps with MW-calibrated infrared estimates. Prior to their use, MW precipitation data are intercalibrated using the reference TRMM Microwave Imager to improve the overall consistency among various MW sensors. Furthermore, T3B42-RT benefits from a TRMM Combined Instrument (TCI) gauge climatological calibration.T3B42 differs from T3B42-RT, as in T3B42 the precipitation data are bias adjusted by scaling the 3-h estimates to sum to a monthly estimate that incorporates monthly gauge data. Furthermore, in T3B42 the TCI from the TRMM 2B31 product (Haddad et al. 1997) is used as a reference for the intercalibration of other MW precipitation estimates. T3B42 is produced at $0.25° \times 0.25°$ spatial resolution every 3 h. CMORPH uses precipitation estimates from MW retrievals exclusively, and produces temporally and spatially complete precipitation fields by interpolating the MW precipitation data along cloud tracks that are obtained entirely from geostationary satellite IR data. CMORPH data are available at $0.25° \times 0.25°$ spatial resolution every 3 h. PERSIANN uses artificial neural networks to establish relationships between infrared and precipitation estimates from a collection of MW products with precipitation rates being estimated directly from IR data. In the adjustment of the network weights, the temporal and regional variabilities in the precipitation data are considered. PERSIANN data are available at $0.25° \times 0.25°$ spatial resolution every hour. CCS is similar to PERSIANN, as it also derives the precipitation rate from IR data. However, unlike PERSIANN, CCS is based on a cloud classification technique: it separates cloud images into distinctive cloud patches, extracts cloud features, clusters cloud patches into well-organized subgroups, and calibrates cloud-top temperature and precipitation relationships for the classified cloud groups. The current CCS dataset does not use MW precipitation data for regular updating of the parameters. The IR–precipitation relationship is based on original training using gauge-corrected radar rainfall data and MW rain estimates. CCS data are produced at $0.04° \times 0.04°$ spatial resolution every half-hour. All of the products were converted to daily and monthly time scales prior to the analysis.

2) GROUND-BASED PRECIPITATING PRODUCTS

Ground-based precipitation products utilized in the study include 1) stage IV radar-based gauge-adjusted precipitation data, available from the National Centers for Environmental Prediction (NCEP), and 2) UW-L13 developed at the University of Washington (UW), which is a gridded dataset of daily meteorological variables (including precipitation, maximum and minimum air temperatures, and wind speed).

The stage IV dataset aggregates the ground radar-derived precipitation data from the National Weather Service River Forecast Centers over the continental United States together with calibration and adjustment for different biases using automated rain gauge measurements and careful quality control processes (Lin and Mitchell 2005). It is available hourly at ~4-km resolution on the Hydrologic Rainfall Analysis Project national grid system.

The UW-L13 dataset includes precipitation, air temperature, and wind speed, as well as humidity and downwelling shortwave and longwave radiation, covering the entire continental United States for the period 1915–2010 at a 3-hourly time step (Livneh et al. 2013). UW-L13 was expanded from a previous dataset (UW-M02; Maurer et al. 2002) that only covered the 1949–2000 period, using the same approach but refining the spatial resolution from $1/8°$ to $1/16°$. The UW-M02 dataset has been used in numerous studies with research foci that ranged from examining the variability of hydroclimatic variables (e.g., Westerling et al. 2006) to downscaling the output of global climate models (e.g., Cayan et al. 2008). The UW-L13 precipitation dataset is derived from in situ measurements at National Climatic Data Center (NCDC) Cooperative Observer stations (DSI3200). Approximately 20 000 stations are used in the product. The Synergraphic Mapping System (SYMAP) interpolation algorithm was applied to grid station data and interpolated onto a $1/16°$ grid, with quality control information (provided by NCDC) incorporated into the gridding process. After interpolation, precipitation was scaled to match the monthly accumulation in the Parameter-Elevation Regressions on Independent Slopes Model (PRISM; Daly et al. 1994) long-term means. Livneh et al. (2013) performed extensive comparisons of simulated hydrologic variables using the UW-L13 dataset to force the VIC model with in situ measurements of soil moisture, radiative and turbulent heat fluxes, snow water equivalent, and runoff, showing good agreement. The UW dataset was used as a reference for daily and monthly analyses. However, as will be shown, UW and STIV produce similar estimates at both time scales.

b. Streamflow observations and other datasets

The other meteorological forcings required by VIC (air temperature and wind speed) are included in the UW-L13 dataset. Gridded maximum and minimum daily air temperatures are produced similarly to precipitation using the SYMAP interpolation algorithm, while wind speed is linearly interpolated from the coarser-scale NCEP–National Center for Atmospheric Research reanalysis product (Kalnay et al. 1996).

Simulated streamflow time series (different for each precipitation product forcing VIC) were evaluated with naturalized streamflow observations that were obtained from the California Data Exchange Center (http://cdec.water.ca.gov). The version of the VIC model used in this study did not account for any anthropogenic effects, hence the reason naturalized streamflow measurements had to be used. The latter are reconstructed from the actual streamflow gauge measurements after adding back the consumptive use for each month (Hidalgo et al. 2009).

3. Results

Analyses are performed for both precipitation inputs and simulated streamflow. The precipitation (UW-L13) and streamflow observations are used as a benchmark for comparative analysis with the other precipitation products and simulated streamflows. Calculations are conducted at each basin and the mean precipitation and streamflow results are compared at monthly and daily time scales. Furthermore, detailed analysis is performed to diagnose sources of error in the remote sensing of precipitation over the region (section 3c).

a. Analysis of precipitation inputs

Figure 2 shows daily precipitation time series (2003–09) for each basin together with the time series of the average precipitation across all basins (shown as a thick black line) for the seven precipitation products. Visual inspection of the UW-L13 and NCEP stage IV (ST4) products (Figs. 2a,b) suggests that the two products agree well in capturing most of the precipitation events, both in terms of their magnitude and timing. The observed similarity is expected because the two products use gauge observations either directly or as a supplement. Gauge data are also used in T3B42, for monthly bias adjustment, as described in section 2a(1). Therefore,

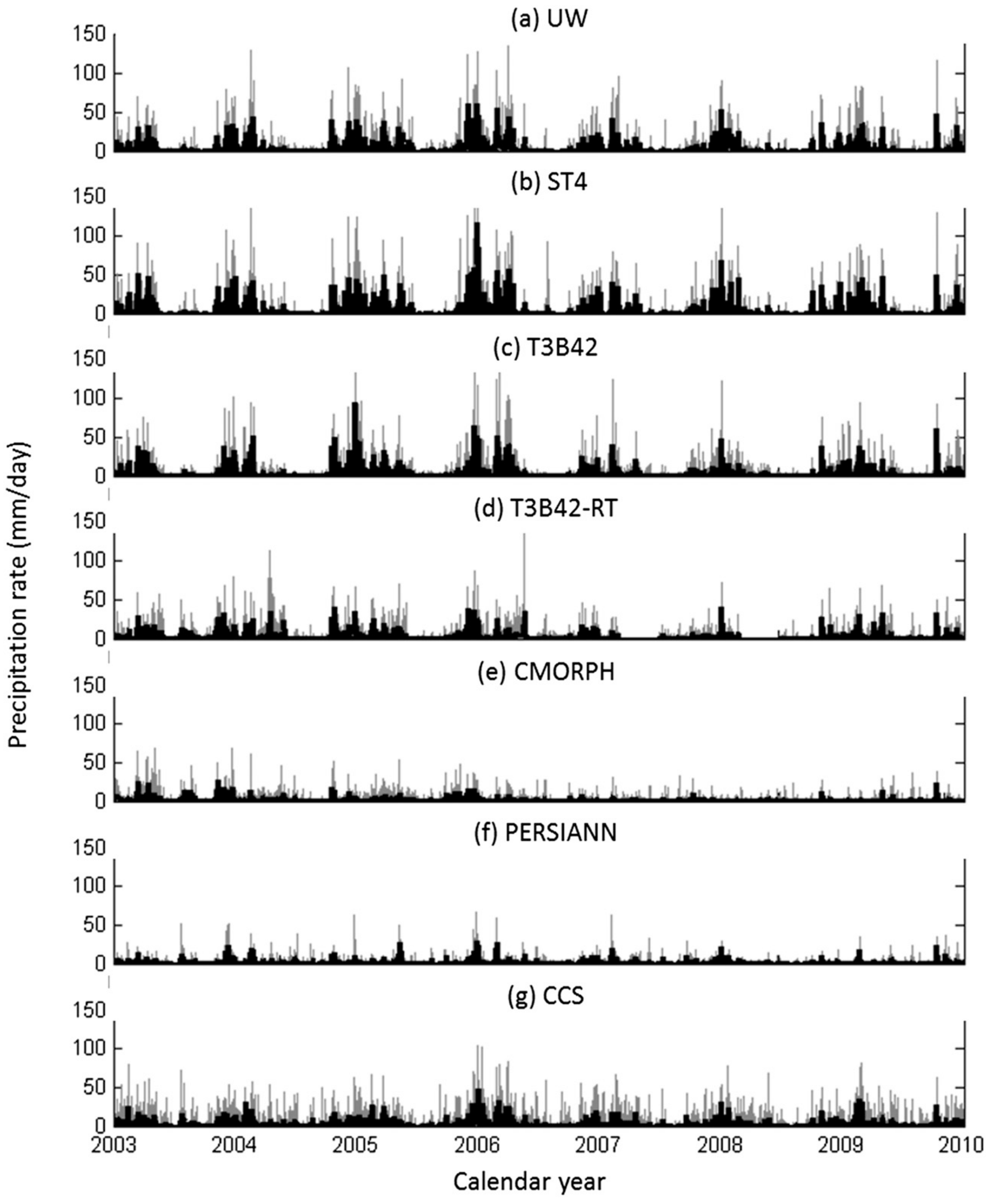

FIG. 2. Daily basin-averaged precipitation time series (2003–09) for each basin (thin vertical gray lines) together with the average of precipitation across all basins (thick black line) from seven products: (a) UW, (b) ST4, (c) T3B42, (d), T3B42-RT, (e) CMORPH, (f) PERSIANN, and (g) CCS. Basins typically show similar precipitation patterns, but with different magnitudes. While daily precipitation time series of individual basins are not easily distinguishable, they collectively display the major differences in the performance of HRPPs.

T3B42 (Fig. 2c) shows higher skill, than the other remote sensing products in capturing precipitation event patterns and magnitudes. The role of gauge adjustment in improving the T3B42 becomes clearer when it is compared with T3B42-RT (Fig. 2d), which does not include gauge adjustment, although the recent version of 3B42-RT (version 7) benefits from some climatology adjustment (Huffman and Bolvin 2014). The other products—CMORPH (Fig. 2e), PERSIANN (Fig. 2f), and CCS (Fig. 2g)—are exclusively based on remote sensing data. CCS outperforms CMORPH and PERSIANN in capturing precipitation event patterns and magnitudes, but it also shows more frequent false precipitation than do the other products. Monthly precipitation time series are shown in Fig. 3, which facilitates intercomparison of the products by focusing on fewer but major precipitation patterns. Similarly, no major differences between the UW-L13 and ST4 products exist, while the gauge-adjusted T3B42 shows relatively good agreement with ST4 and UW-L13. CCS captures the major precipitation patterns, but the other two products (CMORPH and PERSIANN) fail to capture most of the precipitation events. It should be noted that during winter, the precipitation season, more than 1% of the CMORPH data are reported as missing. As will be discussed in section 3b, a large fraction of the missing data can be attributed to precipitation events over frozen surfaces. The missing data are removed in calculating the average precipitation time series (Figs. 2 and 3). However, this could hamper a comparative analysis of CMORPH with the other products. Therefore, CMORPH is not included in the remaining analysis.

Table 1 provides skill scores for the studied products using the UW-L13 precipitation dataset as a benchmark. Corresponding daily and monthly precipitation estimates were collected from all of the basins (shown in Fig. 1) and used to compute the reported skill scores. The results confirm that the ST4 and UW-L13 products are in close agreement, especially on monthly scales (e.g., COR = 0.97, RMSE = 0.97 m day^{-1}, BIASv = 0.95). The bias-adjusted T3B42 performs well on a monthly time scale, but its skill diminishes when comparing daily values. Comparison of T3B42 with T3B42-RT suggests that the bias adjustment is effective and the performance of the product is reduced substantially if no bias adjustment is performed. CCS, an infrared-only technique, outperforms both CMORPH and 3B42-RT at daily and monthly time scales, and shows a bias comparable to T3B42.

The performance of the products is also assessed by binary analysis of daily and monthly precipitation data using a contingency table (Wilks 2011). The construction of the contingency table is based on identifying binary (0/1 or yes/no) events by selecting a precipitation threshold above which a rain event would be considered to have occurred (see the appendix). Figures 4 and 5 demonstrate the ability of the products in capturing the occurrence of precipitation events at a range of precipitation-intensity thresholds. For example, if one considers 1 mm day^{-1} to be a threshold for separating rain from no-rain or major rain from no-major rain, the skill of the products can be assessed using the following metrics: critical success index [CSI; panel a in Figs. 4 and 5], probability of detection (POD; panel b in Figs. 4 and 5), false-alarm ratio (FAR; panel c in Figs. 4 and 5), and BIAS (panel d in Figs. 4 and 5). Capturing the occurrence of precipitation at a range of precipitation rates is important for bias adjustment and assessing the ability of products to capture extreme precipitation events, as well as for improved hydrologic simulations. For example, if precipitation is detected correctly, soil moisture and snowfall can be estimated more reliably, affecting both the timing and intensity of the resulting streamflow simulations.

Figures 4 and 5 suggest that the precipitation detection skill of the products (e.g., based on CSI) diminishes as the precipitation threshold increases. ST4 maintains higher skills (based on CSI and POD) than do the other products across all intensity thresholds, but its FAR increases at more intense precipitation thresholds. The bias-adjusted T3B42 product outperforms other satellite products at the monthly scale. However, at the daily scale the detection performance is comparable to the other products for precipitation intensity less than 5 mm day^{-1}. CCS displays an overall higher skill (e.g., based on CSI) than do T3B42-RT and PERSIANN. Although not bias adjusted using gauges, CCS shows a detection bias comparable to T3B42 that employs bias adjustment using monthly gauge data. Further discussion of the performance of the HRPPs is provided in section 3c. Note that the monthly comparison (Fig. 5) shows only small BIAS between the two products and both monthly BAIS and FAR are fairly independent of the precipitation intensity. This suggests that the algorithmic and instrumental differences used in the UW and ST4 datasets likely cause considerable differences in capturing daily precipitation. Compared to UW precipitation, ST4 shows an underestimation of light and an overestimation of intense precipitation. Arguably, the monthly average of daily precipitation rates can reduce the overall BIAS between the two products. Detailed analysis of the observed differences remains a topic for future research.

b. Evaluation of streamflow predictions

Simulation of streamflow using the VIC model forced by different precipitation products allows further assessment

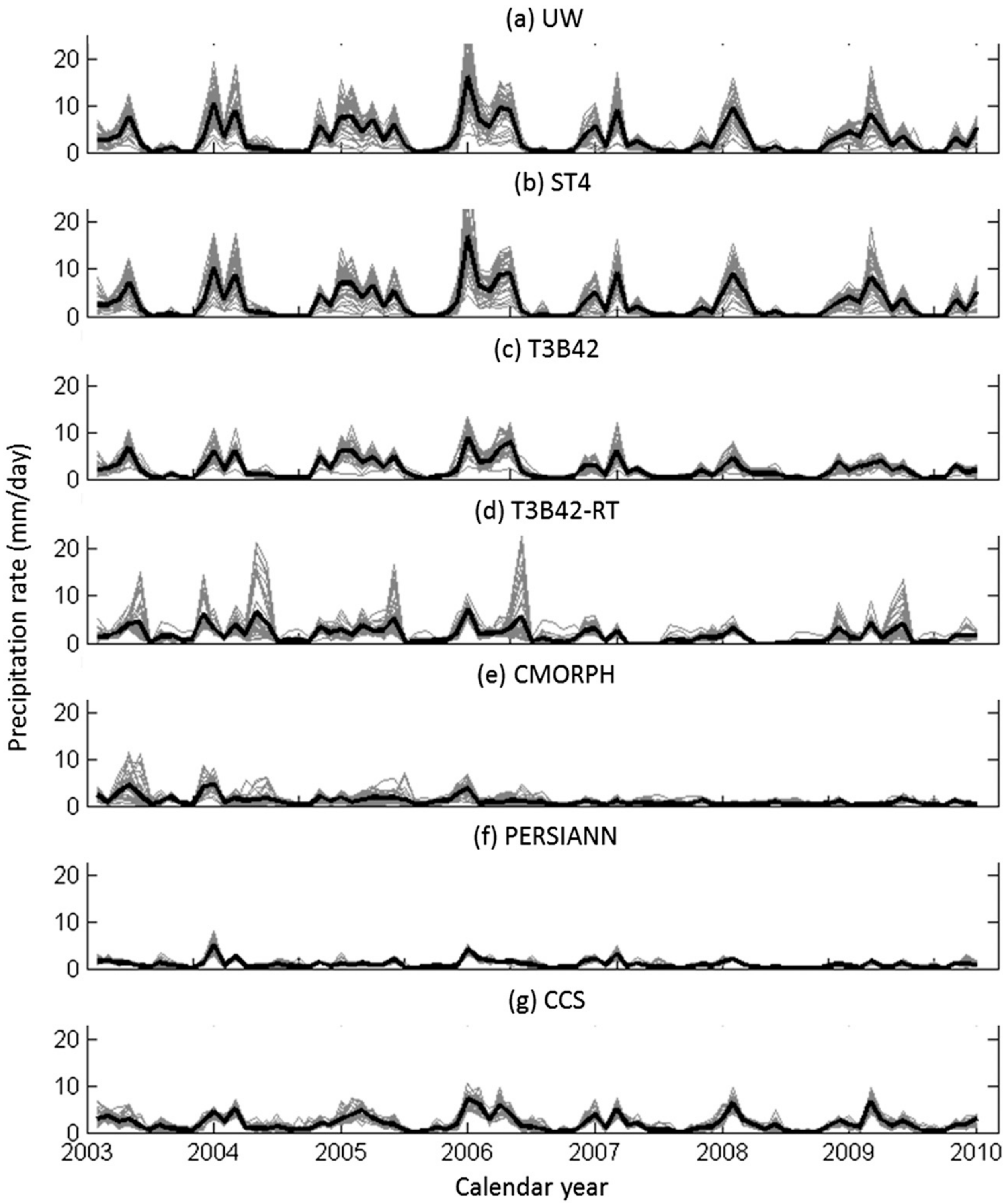

FIG. 3. As in Fig. 2, but for monthly time series.

TABLE 1. A summary of daily and monthly skill scores for precipitation estimates over the studied basins. COR is correlation coefficient, and RMSE is root-mean-square error. BIASv is defined as the ratio of the total estimated to the total observed values with perfection represented by 1. The v in BIASv stands for volume.

	Monthly			Daily		
Products	COR	RMSE (mm day^{-1})	BIASv	COR	RMSE (mm day^{-1})	BIASv
ST4	0.97	0.97	0.95	0.79	5.76	0.95
T3B42	0.86	2.17	0.73	0.55	7.23	0.73
T3B42-RT	0.42	3.55	0.60	0.44	7.39	0.60
CMORPH	0.42	3.78	0.35	0.41	7.46	0.35
PERSIANN	0.72	3.61	0.30	0.50	7.24	0.30
CCS	0.73	2.78	0.65	0.49	7.13	0.65

of the products, especially with respect to their impact on hydrologic prediction linked to many applications (e.g., flood prediction, water resources management, etc.). Through comparison with streamflow observations at basin outlets, the precipitation products can be evaluated indirectly. This evaluation is also important because ground observations of precipitation rate are likely more uncertain in mountainous regions and streamflow, as an integrator of water available on the basin, allows for the overall comparison of the precipitation products.

Figure 6 shows observed monthly streamflow hydrographs (Fig. 6a), as well as those generated by forcing the hydrologic model with the different precipitation products (Figs. 6b–g). Hydrographs for individual basins are shown with thin lines and their average across all the basins is shown with a thick black line. Note that the magnitude of the hydrographs, displayed in Fig. 6, is transformed using the following transformation equation (Hogue et al. 2000; Yilmaz et al. 2005; Behrangi et al. 2011) to enhance the visualization of streamflow peaks along with low flows (e.g., recession parts):

$$\text{Qtrans} = \frac{(Q+1)^{0.6} - 1}{0.6}, \tag{1}$$

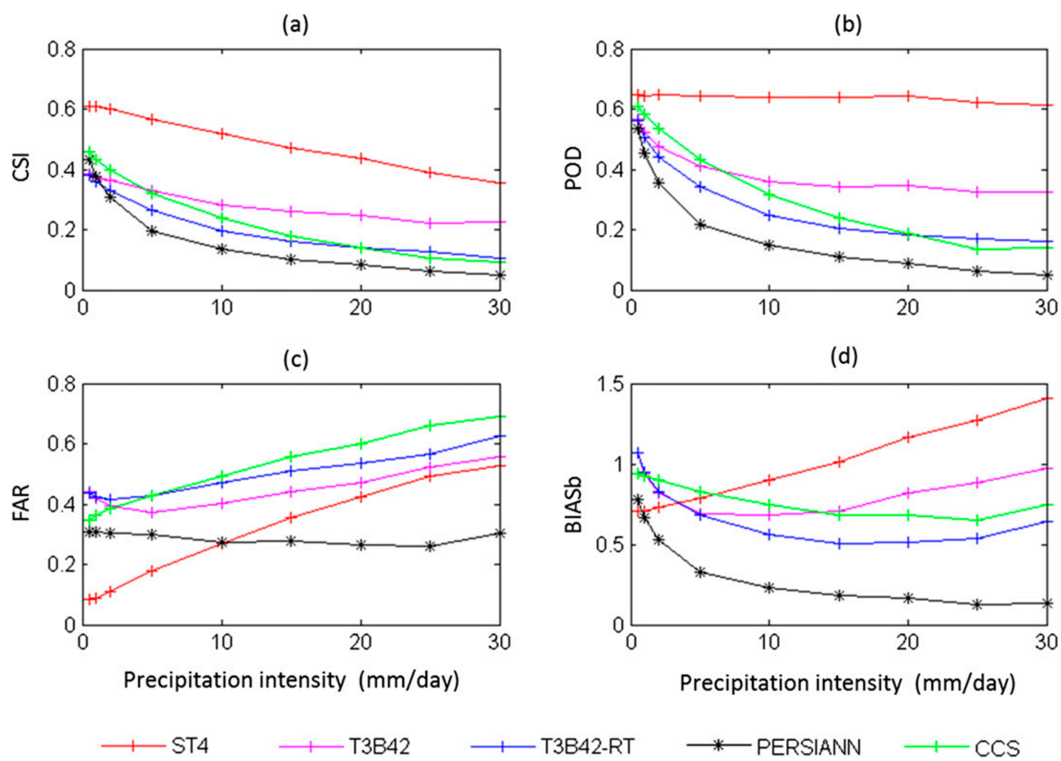

FIG. 4. Binary analysis of daily precipitation from various products using CSI, POD, FAR, and BIASb scores at a range of precipitation intensity thresholds. The binary scores are defined in the appendix. POD, FAR, and CSI range from 0 to 1, with perfection =1 for POD and CSI and 0 for FAR. A BIASb of 1 means that the total number of predicted occurrences is equal to the total number of observed occurrences.

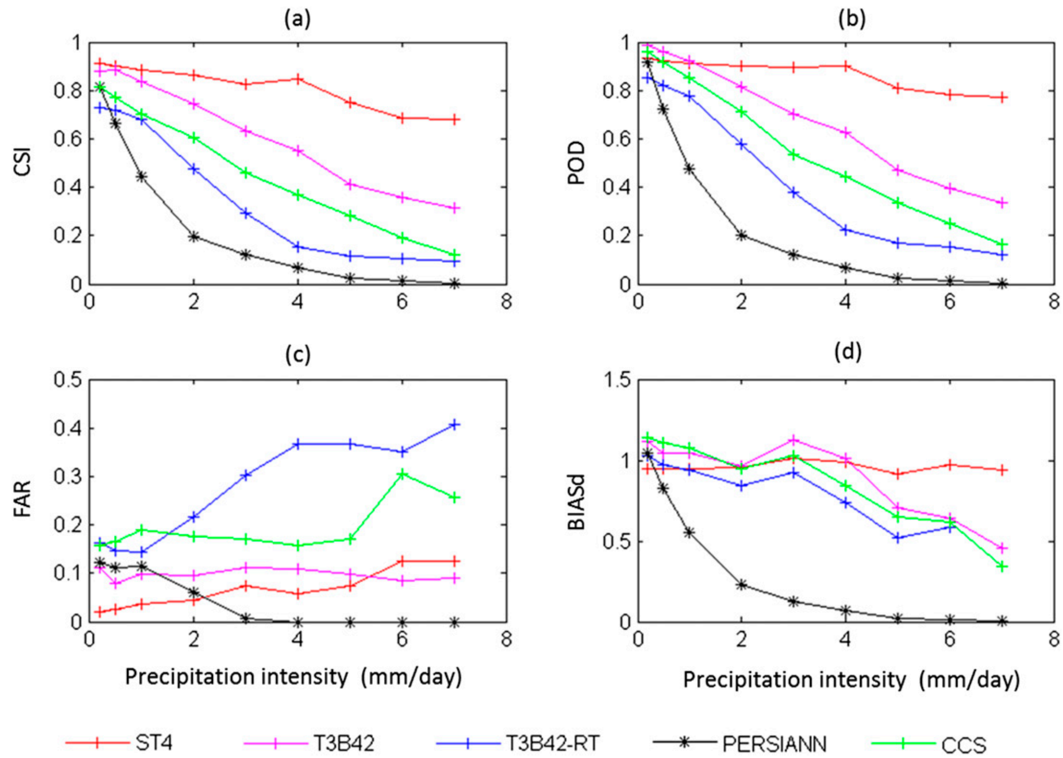

FIG. 5. As in Fig. 4, but at a monthly time scale.

where Qtrans represents streamflow values after transformation from their original value Q.

High similarities (both pattern and magnitude) between observed (Fig. 6a) and simulated streamflows, forced by UW-L13 (Fig. 6b) and ST4 (Fig. 6c) precipitation products, are evident. T3B42-derived streamflows (Fig. 6d) also perform reasonably well in capturing the observed streamflow pattern, but the peak flows are often underestimated. Simulated streamflows forced by CCS, T3B42-RT, and PERSIANN are less skillful, but CCS-derived streamflows seem to outperform those of T3B42-RT and PERSIANN in capturing the magnitudes and patterns of observed streamflows. Further assessment can be obtained using a scatterplot (Fig. 7) of simulated versus observed monthly streamflows, collected from the studied basins. Statistical scores (e.g., COR, RMSE, and BIAS) for monthly and daily time scales are also shown in Table 2 for quantitative comparison. Simulated streamflows forced by UW and ST4 show remarkable skill (COR > 0.9 and BIAS ~ 0.9) compared to streamflow observations. At daily time scales, some of the daily data contain missing values. Therefore, the daily comparisons were conducted using the UW-derived streamflows as a reference. Figure 8 is used to cross-compare the simulated streamflows, forced by different precipitation products, at a range of streamflow thresholds. Notable is the sharp decrease in the skills of the simulated streamflows at higher streamflow thresholds, especially for PERSIANN, CCS, and T3B42-RT. The simulated streamflows from UW and ST4 show almost identical levels of skill with less dependence, compared with the other products, to the streamflow thresholds (except for FAR). Despite monthly bias adjustment employed in T3B42, streamflow simulations forced by T3B42 are not as robust as those forced by the ST4 or UW products. This could be a result of the shortcomings in satellite-based precipitation retrievals, differences in bias-adjustment techniques, or differences in the employed ground observations. However, T3B42 produces a more robust streamflow simulation than does T3B42-RT, suggesting that the employed bias-adjustment technique is valuable.

Results of streamflow analysis are in good agreement with those obtained from analyses of precipitation data. In other words, the results confirm that UW and ST4 are fairly similar and, once used to force the hydrologic model, can produce robust streamflows. Similarly, T3B42 shows significant improvement over T3B42-RT, CCS shows more skill than T3B42-RT, and PERSIANN displays significant underestimation in producing streamflows. While the relatively poor performance for simulating extreme streamflows can be relevant to the choice of hydrologic model and calibration details, a large

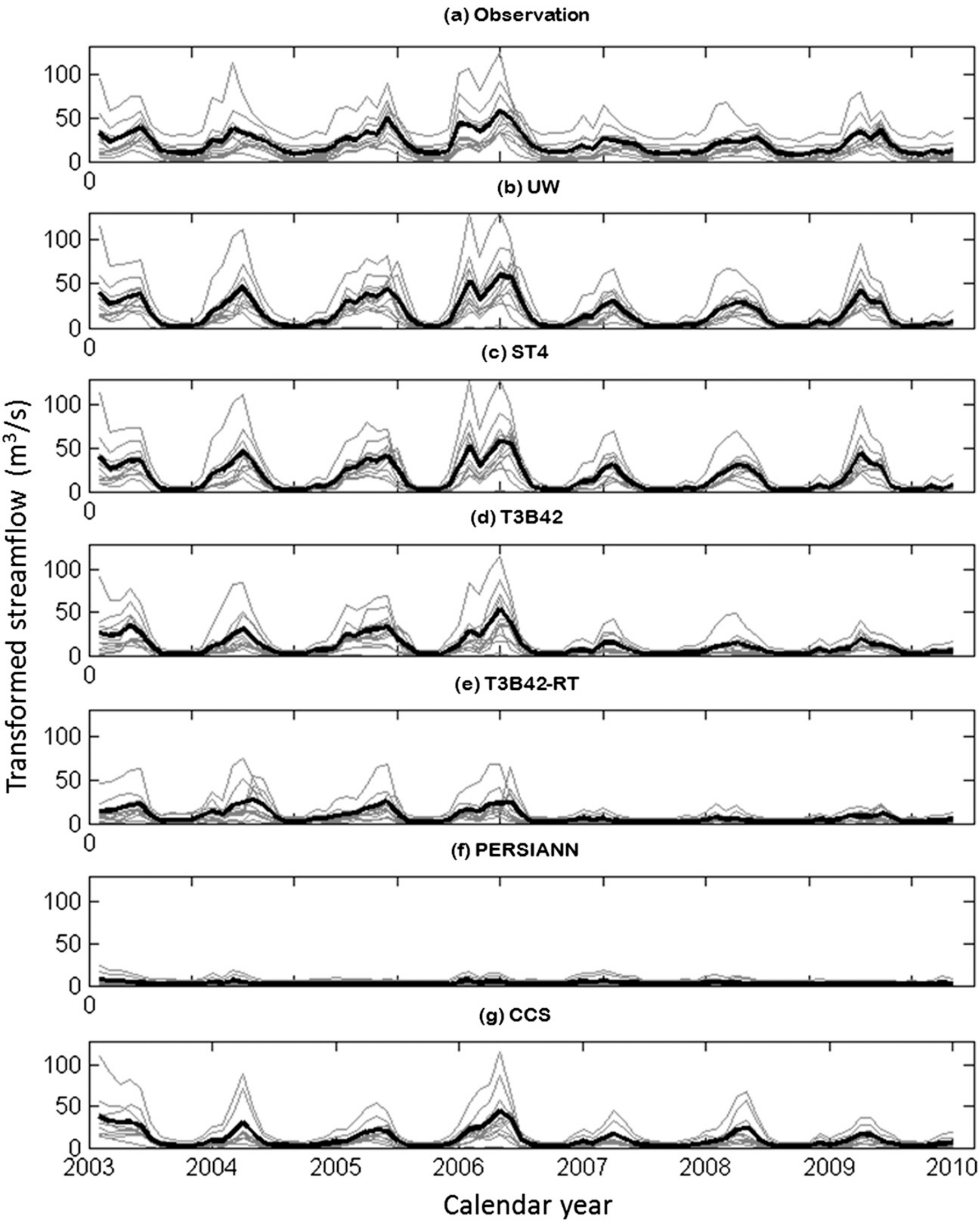

FIG. 6. Monthly streamflow hydrographs from (a) observations, and those generated using (b) UW, (c) ST4, (d) T3B42, (e) T3B42-RT, (f) PERSIANN, and (g) CCS precipitation forcing. A hydrograph of each basin is shown by a thin gray line, and their average across all the basins is shown by a thick black line. The streamflow magnitude (y axis) is transformed using Eq. (1) to improve the visualization.

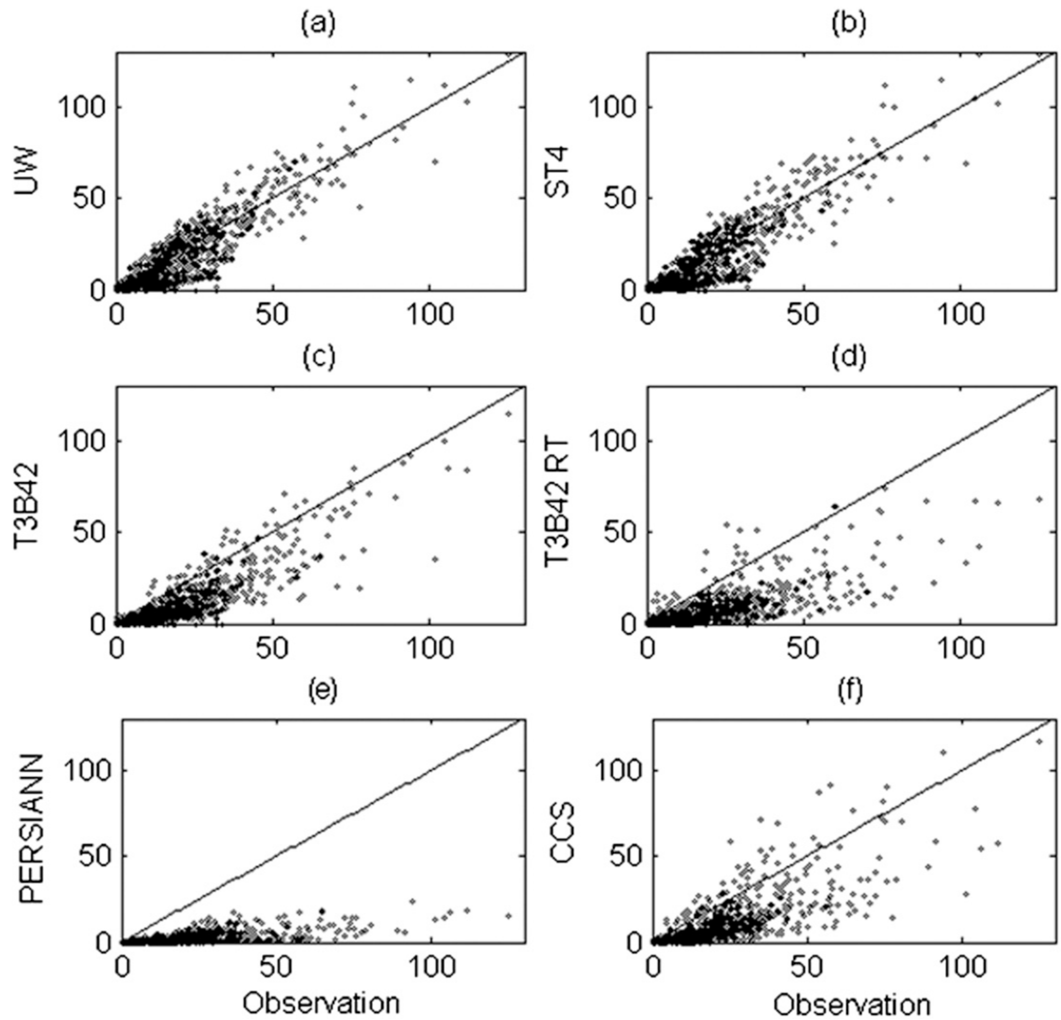

FIG. 7. Scatterplot of observed (x axis) vs simulated (y axis) transformed monthly streamflows ($m^3 s^{-1}$) using various precipitation products: (a) UW, (b) ST4, (c) T3B42, (d) T3B42-RT, (e) PERSIANN, and (f) CCS precipitating forcing. The pairs are collected from the entire studied basins. Transformed streamflows [using Eq. (1)] are plotted to improve the visualization of streamflow peaks along with low flows.

part of it is linked to the skill of the precipitation products in capturing extreme precipitation events as discussed in section 3a.

c. Discussion of the performance of the satellite precipitation products

Remote sensing products are increasingly being used for hydrologic prediction and decision making, especially where ground observations are sparse or nonexistent. The present study suggests that the performance of the precipitation products, exclusively derived from remote sensing data, is not yet satisfactory in mountainous basins. This suggests that more investigations are needed to diagnose the problems and improve the remotely sensed precipitation products. This section extends the previous analysis in an attempt to diagnose potential sources for the observed discrepancies between satellite precipitation products and observations discussed earlier.

Figure 9 shows geographical maps of average seasonal precipitation for different products over a box (35°–43°N and 115°–125°W) that includes the studied basins. From the top to the bottom row the precipitation products are UW, ST4, T3B42, T3B42-RT, CMORPH, PERSIANN, and CCS. The black ellipse, in the top-left panel of Fig. 9, bounds the location of the studied basins (also see Fig. 1). The following points are notable from Fig. 9: 1) the majority of precipitation occurs in winter; 2) average precipitation is intense along the Sierra Nevada because of orographic precipitation; 3) UW and ST4 show strong consistency in capturing the seasonal and regional distributions of precipitation; 4) among the remotely sensed

TABLE 2. A summary of daily and monthly skill scores for streamflow estimates over the studied basins. COR is correlation coefficient, and RMSE is root-mean-square error. BIASv is defined as the ratio of the total estimated to the total observed values, with perfection represented by 1.

	Monthly			Daily*		
Products	COR	RMSE ($m^3 s^{-1}$)	BIASv	COR	RMSE ($m^3 s^{-1}$)	BIASv
UW	0.92	60.44	0.89			
ST4	0.91	62.12	0.88	0.95	18.97	0.97
T3B42	0.86	79.55	0.49	0.88	62.71	0.54
T3B42-RT	0.72	126.15	0.31	0.68	94.34	0.30
CMORPH	0.41	152.74	0.05	0.35	114.43	0.05
PERSIANN	0.66	149.04	0.08	0.62	112.39	0.08
CCS	0.72	103.52	0.42	0.76	0.78	0.47

* Because of a lack of daily streamflow observations, simulation of streamflows using UW precipitation forcing is used as a reference.

products, only T3B42 can reasonably capture the seasonal and regional distributions of precipitation, perhaps due to the implementation of ground-based bias adjustment; 5) while T3B42-RT is less robust than T3B42, it performs more reasonably than do the other precipitation products, exclusively derived from remote sensing data; 6) CMORPH partially captures the regional distribution of precipitation, but shows a significant underestimation of precipitation rate; 7) PERSIANN is not as capable as the other products of capturing the regional and seasonal distributions of precipitation over the region; and 8) CCS reasonably locates mountainous precipitation, but also displays significant false alarms at higher latitudes, especially during the cold months. While the reason for such overestimation has to be investigated in detail, a potential reason could be related to the inability of the infrared data to distinguish between cold surface and cloud-top temperatures.

Careful analysis of CMORPH data over the studied region shows that more than 1% of the observations are missing, especially during winter (Fig. 10). The missing data are mainly due to the missing MW precipitation data from individual sensors, which collectively and exclusively (no IR data) are used in CMORPH. It was

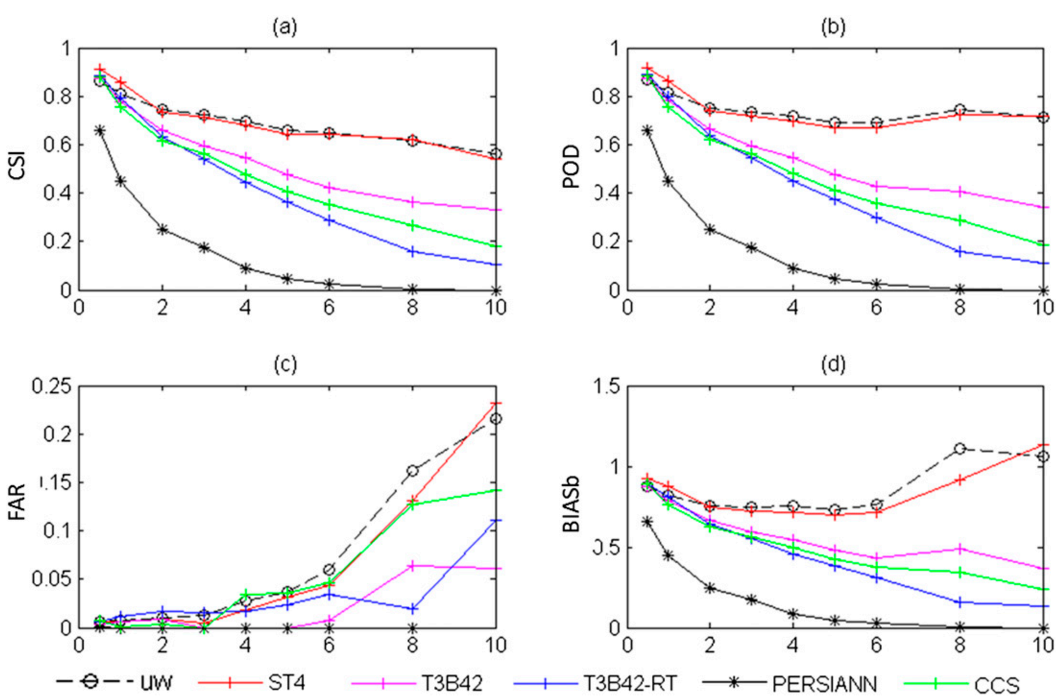

FIG. 8. Binary analysis of monthly streamflow simulations forced by various precipitation products. Comparisons are made for (a) CSI, (b) POD, (c) FAR, and (d) BIASb scores at a range of transformed streamflow thresholds. The binary scores are defined in the appendix.

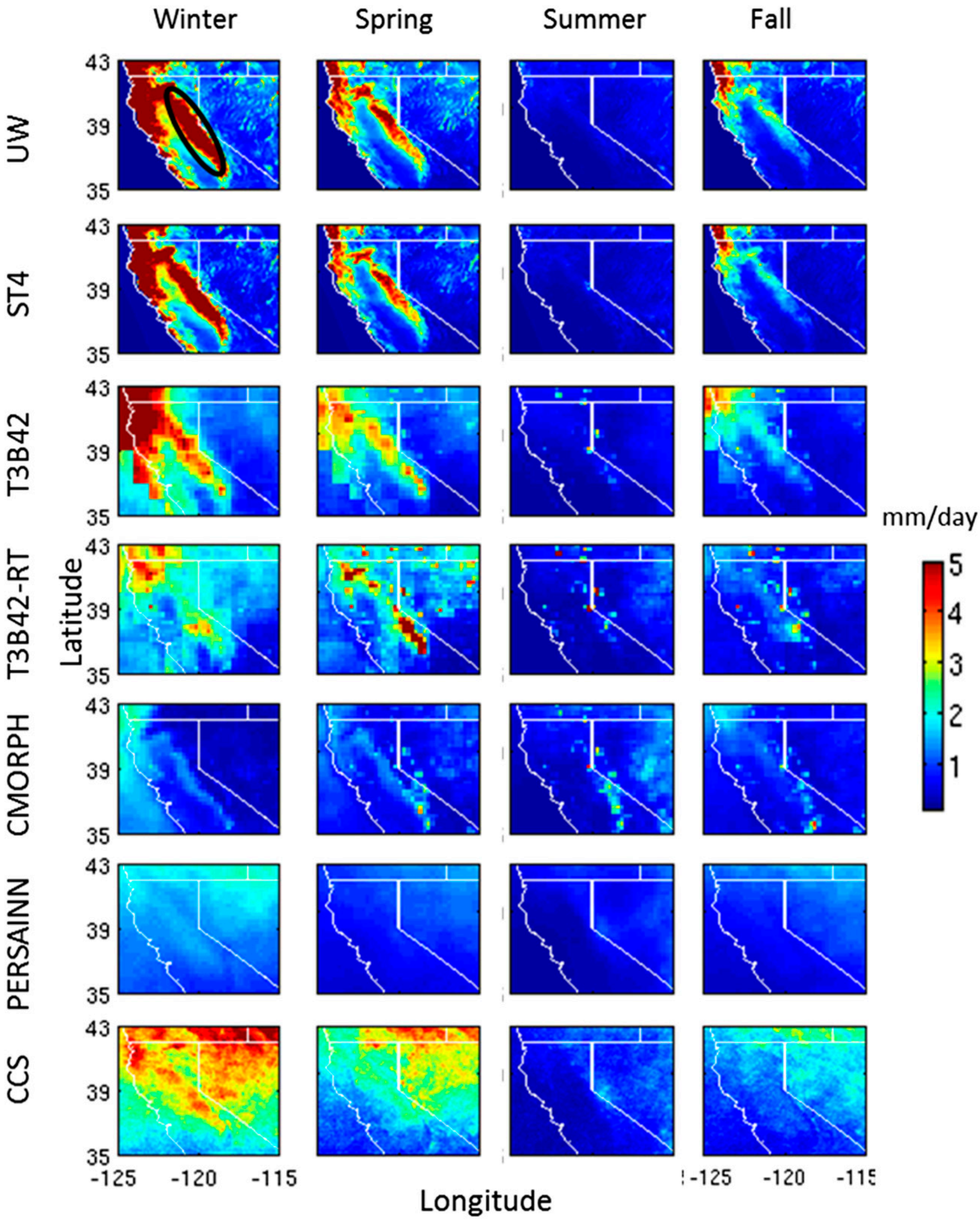

FIG. 9. Geographical maps of average seasonal precipitation for different products.

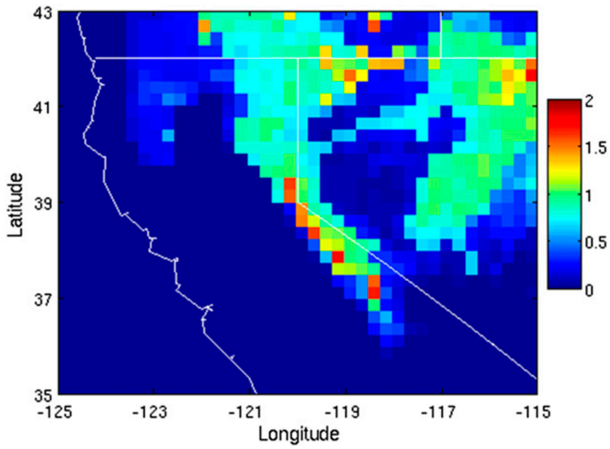

FIG. 10. Frequency (%) of missing data in CMORPH.

also noted that a large fraction of the missing data occurs during precipitation events. In CMORPH the missed MW precipitation data are assigned to zero if no precipitation is inferred from IR images. However, missing data remain for precipitation events over frozen land (R. Joyce 2013, personal communication). This hampers comparative analyses of CMORPH with other products; thus, CMORPH was not included in the analysis described in sections 3a and 3b. T3B42 also depends highly on MW precipitation data, but it fills the missing data with IR-based precipitation estimates. As described in section 2a(1), PERSIANN derives its precipitation results from IR data, and MW precipitation data are only used to adjust the relationship between the IR and precipitation rates. While IR-based precipitation does not typically contain missing values, the quality of the IR precipitation is highly affected by the quality of the MW precipitation, especially when regional training is implemented. This is the case for PERSIANN and T3B41 [T3B41 is an infrared-based rain product used in the production of T3B42; see Huffman et al. (2007)].

Missing data in the MW-derived precipitation dataset occur mainly over snow and frozen surfaces because the current precipitation retrieval techniques from MW observations face difficulties in discriminating the radiometric signal of the precipitation from the underlying surface. This largely impacts the precipitation retrieval from sub-183-GHz-type MW imagers such as the Advanced Microwave Scanning Radiometer for Earth Observing System (AMSR-E; Wilheit et al. 2003) and the Special Sensor Microwave Imager and Sounder (SSM/IS). Precipitation is also retrieved from combinations of channels of the Advanced Microwave Sounding Unit (AMSU) and microwave humidity sounders (MHSs). For example, AMSU/MHS precipitation from the Microwave Surface and Precipitation Products System (Ferraro et al. 2000; Weng et al. 2003; Vila et al. 2007) benefits from a technique (Kongoli et al. 2003) through which a combination of MW sounding channels is used to discriminate the scattering features over land surfaces (especially snow cover) and that of the atmosphere (precipitation-sized ice particles). However, a longstanding difficulty occurs in dry atmospheres (e.g., total water vapor column below 10–15 mm), where even the 183-GHz sounding channels are impacted by the surface.

Figure 11 compares the frequency of precipitation occurrence (Figs. 11a,b), frequency of missing data (Figs. 11c,d), and average precipitation rates (Figs. 11e,f) from AMSR-E (on board *Aqua*, representing MW imagers) and AMSU/MHS [on board the *National Oceanic and Atmospheric Administration-18* (*NOAA-18*) satellite, representing MW sounders] during winter over the studied box (shown in Fig. 9). The two sensors have similar local time observations (~0130/1330 LT at the equator); thus, the diurnal cycle of precipitation does not impact the analysis. As compared with AMSU/MHS, the AMSR-E product misses a significant fraction of the precipitation over land. In contrast, AMSR-E suggests a higher frequency of precipitation over ocean. This is because AMSR-E precipitation retrieval uses a combination of low- and high-frequency channels over the ocean (so it can detect warm rainfall) but mainly relies on the high-frequency channel (e.g., 89 GHz) over land to avoid surface contamination of signals. Therefore, precipitation events that lack ice particles (e.g., warm rainfall that can be produced by low-level atmospheric rivers) are missed. This could be in addition to the missing precipitation events in the presence of snow or ice over land (Fig. 11c). Missing data are also observed in the AMSU/MHS precipitation product, mainly over the north-northeast of Nevada, that are possibly related to the presence of a dry atmosphere. Comparisons of the winter precipitation rate from AMSR-E (Fig. 11e), AMSU/MHS (Fig. 11f), and that from the UW/ST4 products suggest that AMSU/MHS is more robust in producing regional distributions of winter precipitation over land, although it still underestimates the magnitude of precipitation.

It is also important to note that the current precipitation retrieval algorithms over land using MW imagers are almost exclusively limited to rainfall. Therefore, a large fraction of precipitation falling as snowfall can be missed, a considerable problem in the western United States where snowfall dominates the freshwater supply. Figure 12a compares the precipitation detection skill of AMSR-E with that of *CloudSat* as a function of surface elevation. Figure 12 is constructed using collocated AMSR-E and *CloudSat* data over land, during winter (2007–09), and within the studied box shown in Fig. 9.

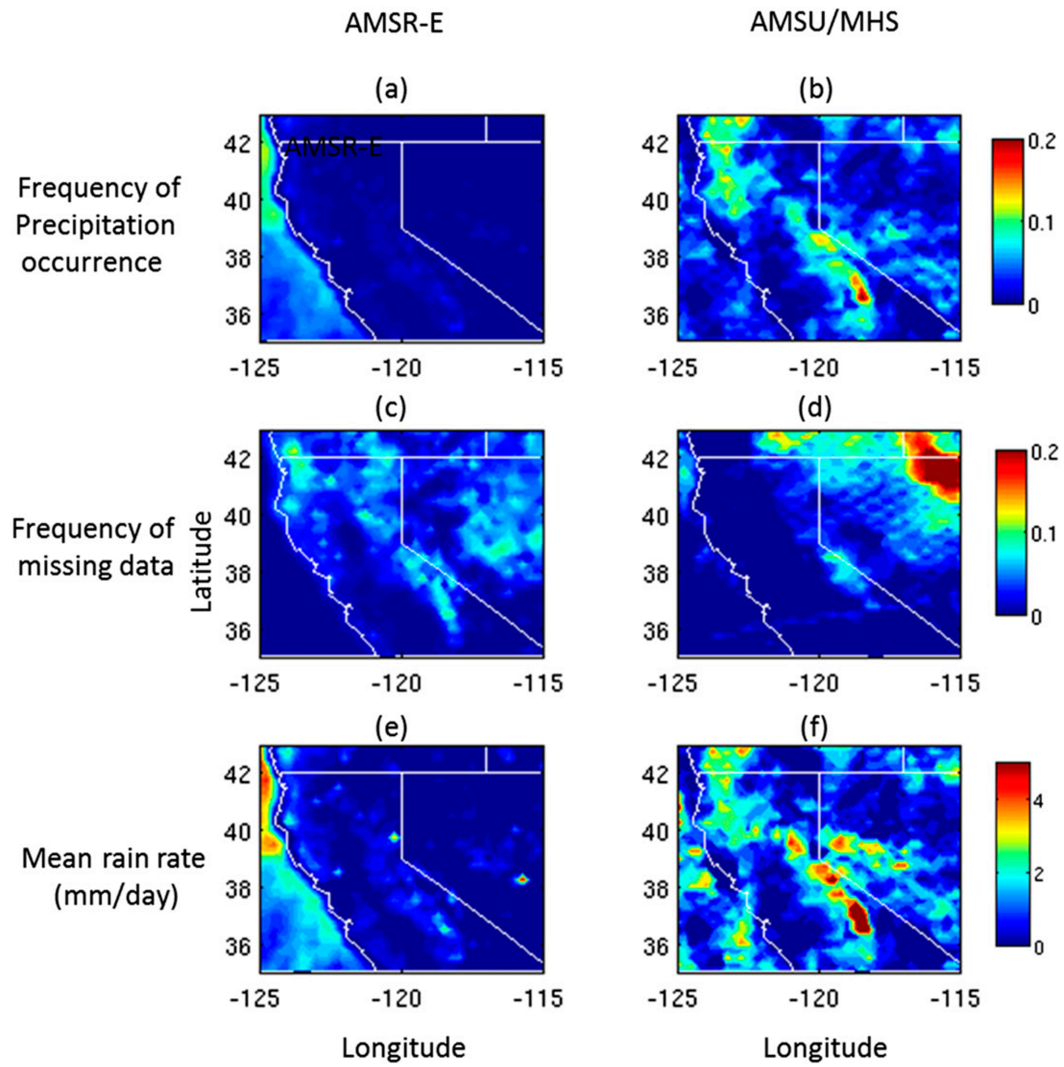

FIG. 11. Comparison of (left) AMSR-E and (right) AMSU/MHS precipitation estimates over the studied region: (a),(b) frequency of precipitation occurrence, (c),(d) frequency of missing data, and (e),(f) average precipitation rates from AMSR-E (on board *Aqua*, representing MW imagers) and AMSU/MHS (on board *NOAA-18*, representing MW sounders) during winter (2007–09).

CloudSat precipitation is obtained from the 2C-PRECIPCOLUMN product (Haynes et al. 2009) and is shown for different precipitation phases (rain, snow, and mixed phase). The product provides flags of ''possible,'' ''probable,'' and ''certain'' precipitation occurrence for rain, snow, and mixed-phase precipitation. Only certain precipitation flags are used in our analysis. Note that when precipitation forms below about 720 m, contamination from ground clutter may prevent the detection of rain in the 2C-PRECIPCOLUMN product. Sample counts are also shown in Fig. 12b. The high sensitivity of the *CloudSat* Cloud Profiling Radar to liquid and frozen hydrometeors enables superior estimates of light rain and snowfall, which goes undetected by other sensors (Behrangi et al. 2012; Behrangi et al. 2014; Smalley et al. 2014). Clearly, a major fraction of precipitation is missed by the AMSR-E precipitation product, especially at higher elevations where snowfall is the dominant type of precipitation.

4. Concluding remarks

The performance of several commonly used satellite-combined precipitation products (HRPPs) in estimating observed precipitation and streamflow are investigated over the mountainous San Joaquin–Sacramento basins (Fig. 1). A large fraction of the annual precipitation over the studied basins occurs during winter (Figs. 2 and 3),

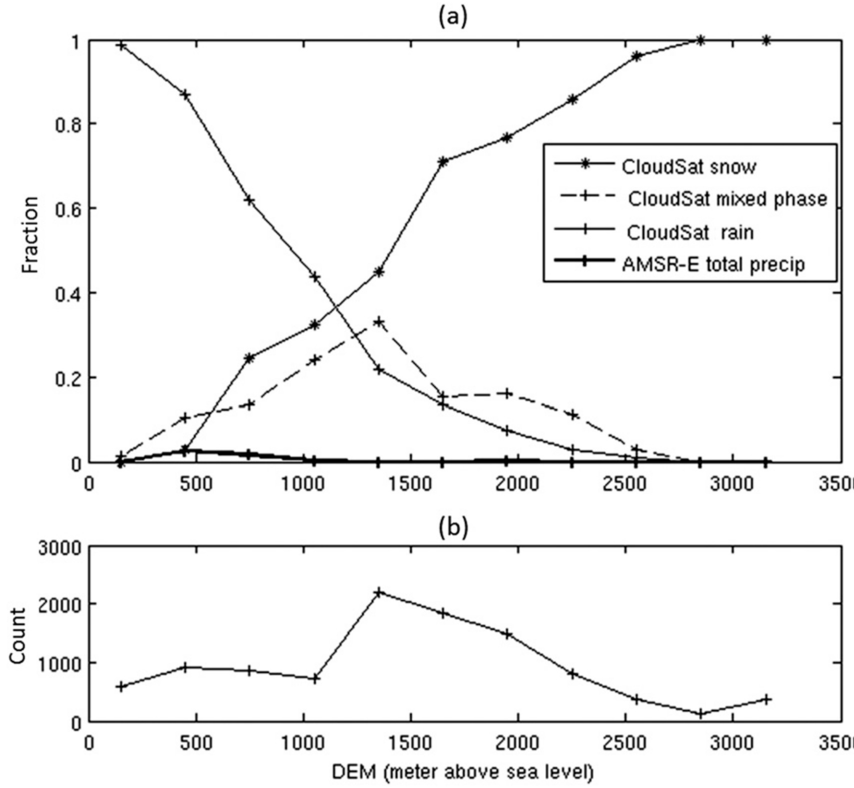

FIG. 12. Comparison of *CloudSat* and AMSR-E precipitation detection results using collocated data over land from three winter seasons (2007–09). (a) Fraction of total precipitation observed by *CloudSat*. (b) Count of collocated data used for analysis. In (a), the fractions of *CloudSat* rain, snow, and mixed-phase precipitation sum to 1 at each elevation bin.

often with substantial snowfall at high elevations (Fig. 12). Streamflows are simulated by forcing the Variable Infiltration Capacity hydrological model with HRPPs. Most of the HRPPs and simulated streamflows capture major precipitation patterns. However, the study suggests that the performance of HRPPs is not yet satisfactory in mountainous basins, especially if not adjusted for bias using ground observations. Precipitation is typically not well detected and the intensities are often significantly underestimated (e.g., Figs. 4 and 5). As precipitation is the major forcing for hydrologic simulations, the observed errors are well propagated and manifested in simulated streamflows (Figs. 6–8) that can negatively impact several applications such as water resource management and flood control. The high similarity between precipitation and streamflow errors suggests that significant improvement in streamflow simulation is possible if higher quality HRPPs are obtained.

Recognizing that a majority of global mountainous basins lack ground observations, HRPPs remain a main observational source for quantifying precipitation and deriving hydrologic products for applications and societal benefit. Detailed investigations show that the performance of HRPPs is tightly linked to the precipitation retrievals from individual sensors. Currently, the precipitation retrieval technique faces major difficulties in retrieving snowfall and warm rainfall (Fig. 12; also see Behrangi et al. 2012). Precipitation over frozen land is also challenging and at the present time results in missing data in microwave precipitation products, especially from microwave imagers (Figs. 10 and 11), which negatively impacts the HRPPs (Fig. 10). Precipitation retrievals from microwave sounder and infrared data can produce more reasonable precipitation estimates over the studied region, but the indirect infrared techniques often show poor detection skill, and microwave sounding in dry atmosphere remains challenging. This calls for more rigorous effort to diagnose the problems directly at level 2 (orbital data products), especially over regions that experience snowfall, as well as cold or snow-covered surfaces. Understanding the error characteristics of level-2 products is also critical to designing more appropriate combination techniques for the production of HRPPs.

In the near future, the joint NASA–Japanese Aerospace Exploration Agency (JAXA) Global Precipitation Measurement mission will deploy a dual-frequency Ka–Ku-band precipitation radar (DPR) on its ''core'' satellite, covering ocean and land surfaces between 65°S and 65°N. Data from the DPR should improve the ability to distinguish precipitation phases and provide better descriptions of the hydrometeor size distribution needed for the level 2 precipitation products from the constellation of satellites (which are the main microwave inputs to the HRPPs). Also, the overland precipitation retrieval techniques will be more physically based, taking into account surface characteristics (Kummerow et al. 2011; Ferraro et al. 2013). The GPM mission together with these improved precipitation retrieval algorithms will create an unprecedented opportunity to improve the global quantification of precipitation and its characteristics and by extension hydrologic predictions, especially over higher latitudes and cold regions.

Acknowledgments. Funding for this research came from a JPL Research and Technology Development investment (RHEAS). This study was also supported by the NASA New (Early Career) Investigator Program in Earth Science (NNH13ZDA001N-NIP) and NASA Weather (NNH13ZDA001N-WEATHER) awards. The research described in this paper was carried out at the Jet Propulsion Laboratory, California Institute of Technology, under a contract with the National Aeronautics and Space Administration. Government sponsorship is acknowledged.

APPENDIX

Binary Scores Based on a Contingency Table

Using observed and estimated–predicted data, a contingency table can be constructed to classify the predictions–estimates into the following four possibilities based on binary (1/0 or yes/no) occurrences (e.g., rain/no rain):

1) hit (H)—number of events correctly classified as having occurred (e.g., rain),
2) miss (M)—number of events incorrectly classified as not having occurred (e.g., no rain),
3) false alarm (F)—number of events incorrectly classified as having occurred (e.g., rain), and
4) correct negative (Z)—number of events correctly classified as not having occurred (e.g., no rain).

A perfect predictor would produce only hits and correct negatives and no misses or false alarms, but prediction systems are not always perfect. The contingency table can be used to derive the following scores that are commonly used to evaluate the prediction skills of the models:

- probability of detection: $\mathrm{POD} = H/(H + m)$,
- false-alarm ratio: $\mathrm{FAR} = F/(H + F)$,
- BIAS: $\mathrm{BIASb} = (H + F)/(H + M)$, where b stands for binary, and
- critical success index: $\mathrm{CSI} = H/(H + F + M)$.

POD, FAR, and CSI range from 0 to 1, with perfection represented by 1 for POD and CSI and 0 for FAR. POD is sensitive to the number of hits, but it ignores false alarms; FAR, on the other hand, is sensitive to false alarms, but it ignores misses. CSI takes into account both false alarms and missed events and, unlike the POD and the FAR, is a more balanced score. BIAS considers both predictions and observations. A BIAS of 1 means that the total number of predicted occurrences ($H + F$) is equal to the total number of observed occurrences. However, a perfect BIAS score of 1 does not necessarily indicate a perfect skill of the predictor.

REFERENCES

Andreadis, K. M., E. A. Clark, A. W. Wood, A. F. Hamlet, and D. P. Lettenmaier, 2005: Twentieth-century drought in the conterminous United States. *J. Hydrometeor.,* **6,** 985–1001, doi:10.1175/JHM450.1.

Baird, B. P., and R. R. Robles, 1997: Emergency management issues in the California floods of 1997: Lessons learned or lessons lost? California Specialized Training Institute Doc. G4173 N3, San Luis Obispo, CA, 54 pp. [Available from California Specialized Training Institute, P.O. Box 8123, San Luis Obispo, CA 93403-8123.]

Behrangi, A., K. Hsu, B. Imam, S. Sorooshian, G. J. Huffman, and R. J. Kuligowski, 2009: PERSIANN-MSA: A precipitation estimation method from satellite-based multispectral analysis. *J. Hydrometeor.,* **10,** 1414–1429, doi:10.1175/2009JHM1139.1.

——, ——, ——, ——, and ——, 2010: Daytime precipitation estimation using bispectral cloud classification system. *J. Appl. Meteor. Climatol.,* **49,** 1015–1031, doi:10.1175/2009JAMC2291.1.

——, B. Khakbaz, T. C. Jaw, A. AghaKouchak, K. Hsu, and S. Sorooshian, 2011: Hydrologic evaluation of satellite precipitation products over a mid-size basin. *J. Hydrol.,* **397,** 225–237, doi:10.1016/j.jhydrol.2010.11.043.

——, M. Lebsock, S. Wong, and B. Lambrigtsen, 2012: On the quantification of oceanic rainfall using spaceborne sensors. *J. Geophys. Res.,* **117,** D20105, doi:10.1029/2012JD017979.

——, G. Stephens, R. F. Adler, G. J. Huffman, B. Lambrigtsen, and M. Lebsock, 2014: An update on the oceanic precipitation rate and its zonal distribution in light of advanced observations from space. *J. Climate,* **27,** 3957–3965, doi:10.1175/JCLI-D-13-00679.1.

Berg, W., T. L'Ecuyer, and C. Kummerow, 2006: Rainfall climate regimes: The relationship of regional TRMM rainfall biases to the environment. *J. Appl. Meteor. Climatol.,* **45,** 434–454, doi:10.1175/JAM2331.1.

Bitew, M. M., M. Gebremichael, L. T. Ghebremichael, and Y. A. Bayissa, 2012: Evaluation of high-resolution satellite rainfall products through streamflow simulation in a hydrological modeling of a small mountainous watershed in Ethiopia. *J. Hydrometeor.,* **13,** 338–350, doi:10.1175/2011JHM1292.1.

Cayan, D., E. Maurer, M. Dettinger, M. Tyree, and K. Hayhoe, 2008: Climate change scenarios for the California region. *Climatic Change,* **87,** 21–42, doi:10.1007/s10584-007-9377-6.

Daly, C., R. P. Neilson, and D. L. Phillips, 1994: A statistical–topographic model for mapping climatological precipitation over mountainous terrain. *J. Appl. Meteor.,* **33,** 140–158, doi:10.1175/1520-0450(1994)033<0140:ASTMFM>2.0.CO;2.

Defries, R. S., M. C. Hansen, J. R. G. Townshend, A. C. Janetos, and T. R. Loveland, 2000: A new global 1-km dataset of percentage tree cover derived from remote sensing. *Global Change Biol.,* **6,** 247–254, doi:10.1046/j.1365-2486.2000.00296.x.

Dettinger, M., 2011: Climate change, atmospheric rivers, and floods in California—A multimodel analysis of storm frequency and magnitude changes1. *J. Amer. Water Resour. Assoc.,* **47,** 514–523, doi:10.1111/j.1752-1688.2011.00546.x.

Dinku, T., P. Ceccato, K. Cressman, and S. J. Connor, 2010: Evaluating detection skills of satellite rainfall estimates over desert locust recession regions. *J. Appl. Meteor. Climatol.,* **49,** 1322–1332, doi:10.1175/2010JAMC2281.1.

Ebert, E. E., J. E. Janowiak, and C. Kidd, 2007: Comparison of near-real-time precipitation estimates from satellite observations and numerical models. *Bull. Amer. Meteor. Soc.,* **88,** 47–64, doi:10.1175/BAMS-88-1-47.

Ferraro, R. R., N. Grody, and G. Marks, 1994: Effects of surface conditions on rain identification using the DMSP-SSM/I. *Remote Sens. Rev.,* **11,** 195–209, doi:10.1080/02757259409532265.

——, F. H. Weng, N. C. Grody, and L. M. Zhao, 2000: Precipitation characteristics over land from the *NOAA-15* AMSU sensor. *Geophys. Res. Lett.,* **27,** 2669–2672, doi:10.1029/2000GL011665.

——, and Coauthors, 2005: NOAA operational hydrological products derived from the advanced microwave sounding unit. *IEEE Trans. Geosci. Remote Sens.,* **43,** 1036–1049.

——, and Coauthors, 2013: An evaluation of microwave land surface emissivities over the continental United States to benefit GPM-Era precipitation algorithms. *IEEE Trans. Geosci. Remote Sens.,* **51,** 378–398.

Gebregiorgis, A. S., Y. Tian, C. D. Peters-Lidard, and F. Hossain, 2012: Tracing hydrologic model simulation error as a function of satellite rainfall estimation bias components and land use and land cover conditions. *Water Resour. Res.,* **48,** W11509, doi:10.1029/2011WR011643.

Gopalan, K., N.-Y. Wang, R. Ferraro, and C. Liu, 2010: Status of the TRMM 2A12 land precipitation algorithm. *J. Atmos. Oceanic Technol.,* **27,** 1343–1354, doi:10.1175/2010JTECHA1454.1.

Guan, B., N. P. Molotch, D. E. Waliser, E. J. Fetzer, and P. J. Neiman, 2010: Extreme snowfall events linked to atmospheric rivers and surface air temperature via satellite measurements. *Geophys. Res. Lett.,* **37,** L20401, doi:10.1029/2010GL044696.

Haddad, Z. S., E. A. Smith, C. D. Kummerow, T. Iguchi, M. R. Farrar, S. L. Durden, M. Alves, and W. S. Olson, 1997: The TRMM ''day-1'' radar/radiometer combined rain-profiling algorithm. *J. Meteor. Soc. Japan,* **75,** 799–809.

Haynes, J. M., T. S. L'Ecuyer, G. L. Stephens, S. D. Miller, C. Mitrescu, N. B. Wood, and S. Tanelli, 2009: Rainfall retrieval over the ocean with spaceborne W-band radar. *J. Geophys. Res.,* **114,** D00A22, doi:10.1029/2008JD009973.

Hidalgo, H. G., and Coauthors, 2009: Detection and attribution of streamflow timing changes to climate change in the western United States. *J. Climate,* **22,** 3838–3855, doi:10.1175/2009JCLI2470.1.

Hogue, T. S., S. Sorooshian, H. Gupta, A. Holz, and D. Braatz, 2000: A multistep automatic calibration scheme for river forecasting models. *J. Hydrometeor.,* **1,** 524–542, doi:10.1175/1525-7541(2000)001<0524:AMACSF>2.0.CO;2.

Hong, Y., K. L. Hsu, S. Sorooshian, and X. G. Gao, 2004: Precipitation estimation from remotely sensed imagery using an artificial neural network cloud classification system. *J. Appl. Meteor.,* **43,** 1834–1852, doi:10.1175/JAM2173.1.

——, R. F. Adler, F. Hossain, S. Curtis, and G. J. Huffman, 2007: A first approach to global runoff simulation using satellite rainfall estimation. *Water Resour. Res.,* **43,** W08502, doi:10.1029/2006WR005739.

Hossain, F., and E. N. Anagnostou, 2004: Assessment of current passive-microwave- and infrared-based satellite rainfall remote sensing for flood prediction. *J. Geophys. Res.,* **109,** D07102, doi:10.1029/2003JD003986.

Hou, A. Y., and Coauthors, 2013: The Global Precipitation Measurement (GPM) mission. *Bull. Amer. Meteor. Soc.,* **95,** 701–722, doi:10.1175/BAMS-D-13-00164.1.

Hsu, K. L., X. G. Gao, S. Sorooshian, and H. V. Gupta, 1997: Precipitation estimation from remotely sensed information using artificial neural networks. *J. Appl. Meteor.,* **36,** 1176–1190, doi:10.1175/1520-0450(1997)036<1176:PEFRSI>2.0.CO;2.

Huffman, G. J., and D. T. Bolvin, 2014: TRMM and other data precipitation data set documentation. NASA GSFC, 42 pp. [Available online at ftp://precip.gsfc.nasa.gov/pub/trmmdocs/3B42_3B43_doc.pdf.]

——, and Coauthors, 2007: The TRMM Multisatellite Precipitation Analysis (TMPA): Quasi-global, multiyear, combined-sensor precipitation estimates at fine scales. *J. Hydrometeor.,* **8,** 38–55, doi:10.1175/JHM560.1.

——, D. Bolvin, D. Braithwaite, K. Hsu, R. Joyce, and P. P. Xie, 2013: Integrated Multi-satellite Retrievals for GPM (IMERG), algorithm theoretical basis document (ATBD), version 4.1. NASA, 25 pp. [Available online at http://pmm.nasa.gov/sites/default/files/document_files/IMERG_ATBD_V4.1.pdf .]

Kongoli, C., P. Pellegrino, R. R. Ferraro, N. C. Grody, and H. Meng, 2003: A new snowfall detection algorithm over land using measurements from the Advanced Microwave Sounding Unit (AMSU). *Geophys. Res. Lett.,* **30,** 1756, doi:10.1029/2003GL017177.

Joyce, R. J., J. E. Janowiak, P. A. Arkin, and P. Xie, 2004: CMORPH: A method that produces global precipitation estimates from passive microwave and infrared data at high spatial and temporal resolution. *J. Hydrometeor.,* **5,** 487–503, doi:10.1175/1525-7541(2004)005<0487:CAMTPG>2.0.CO;2.

Kalnay, E., and Coauthors, 1996: The NCEP/NCAR 40-Year Reanalysis Project. *Bull. Amer. Meteor. Soc.,* **77,** 437–471, doi:10.1175/1520-0477(1996)077<0437:TNYRP>2.0.CO;2.

Kidd, C., P. Bauer, J. Turk, G. J. Huffman, R. Joyce, K. L. Hsu, and D. Braithwaite, 2012: Intercomparison of high-resolution precipitation products over northwest Europe. *J. Hydrometeor.,* **13,** 67–83, doi:10.1175/JHM-D-11-042.1.

——, E. Dawkins, and G. Huffman, 2013: Comparison of precipitation derived from the ECMWF operational forecast model and satellite precipitation datasets. *J. Hydrometeor.,* **14,** 1463–1482, doi:10.1175/JHM-D-12-0182.1.

Krakauer, N., S. Pradhanang, T. Lakhankar, and A. Jha, 2013: Evaluating satellite products for precipitation estimation in mountain regions: A case study for Nepal. *Remote Sens.,* **5,** 4107–4123, doi:10.3390/rs5084107.

Kucera, P., and B. Lapeta, 2013: IPWG recent accomplishments and future directions. Expert Team on Satellite Utilization and Products (ET-SUP 7), Coordination Group for Meteorological Satellites (CGMS), Geneva, Switzerland, 13 pp. [Available online at http://www.wmo.int/pages/prog/sat/meetings/documents/ET-SUP-7_Doc_15-02_IPWG.pdf.]

——, E. E. Ebert, F. J. Turk, V. Levizzani, D. Kirschbaum, F. J. Tapiador, A. Loew, and M. Borsche, 2013: Precipitation from space: Advancing earth system science. *Bull. Amer. Meteor. Soc.,* **94,** 365–375, doi:10.1175/BAMS-D-11-00171.1.

Kuligowski, R. J., 2002: A self-calibrating real-time GOES rainfall algorithm for short-term rainfall estimates. *J. Hydrometeor.,* **3,** 112–130, doi:10.1175/1525-7541(2002)003<0112:ASCRTG>2.0.CO;2.

Kummerow, C. D., S. Ringerud, J. Crook, D. Randel, and W. Berg, 2011: An observationally generated a priori database for microwave rainfall retrievals. *J. Atmos. Oceanic Technol.,* **28,** 113–130, doi:10.1175/2010JTECHA1468.1.

Lebsock, M. D., and T. S. L'Ecuyer, 2011: The retrieval of warm rain from *CloudSat*. *J. Geophys. Res.,* **116,** D20209, doi:10.1029/2011JD016076.

Liang, X., and Z. Xie, 2001: A new surface runoff parameterization with subgrid-scale soil heterogeneity for land surface models. *Adv. Water Resour.,* **24,** 1173–1193, doi:10.1016/S0309-1708(01)00032-X.

——, D. P. Lettenmaier, and E. F. Wood, 1996: One-dimensional statistical dynamic representation of subgrid spatial variability of precipitation in the two-layer variable infiltration capacity model. *J. Geophys. Res.,* **101,** 21 403–21 422, doi:10.1029/96JD01448.

Lin, Y., and K. E. Mitchell, 2005: The NCEP stage II/IV hourly precipitation analyses: Development and applications. *19th Conf. on Hydrology,* San Diego, CA, Amer. Meteor. Soc., 1.2. [Available online at https://ams.confex.com/ams/pdfpapers/83847.pdf.]

Livneh, B., E. A. Rosenberg, C. Lin, B. Nijssen, V. Mishra, K. M. Andreadis, E. P. Maurer, and D. P. Lettenmaier, 2013: A long-term hydrologically based dataset of land surface fluxes and states for the conterminous United States: Update and extensions. *J. Climate,* **26,** 9384–9392, doi:10.1175/JCLI-D-12-00508.1.

Lohmann, D., E. Raschke, B. Nijssen, and D. P. Lettenmaier, 1998: Regional scale hydrology: I. Formulation of the VIC-2L model coupled to a routing model. *Hydrol. Sci. J.,* **43,** 131–141, doi:10.1080/02626669809492107.

——, and Coauthors, 2004: Streamflow and water balance intercomparisons of four land surface models in the North American Land Data Assimilation System project. *J. Geophys. Res.,* **109,** D07S91, doi:10.1029/2003JD003517.

Maurer, E. P., A. W. Wood, J. C. Adam, D. P. Lettenmaier, and B. Nijssen, 2002: A long-term hydrologically based dataset of land surface fluxes and states for the conterminous United States. *J. Climate,* **15,** 3237–3251, doi:10.1175/1520-0442(2002)015<3237:ALTHBD>2.0.CO;2.

Miller, D. A., and R. A. White, 1998: A conterminous United States multilayer soil characteristics dataset for regional climate and hydrology modeling. *Earth Interact.,* **2,** doi:10.1175/1087-3562(1998)002<0001:ACUSMS>2.3.CO;2.

Neiman, P. J., F. M. Ralph, G. A. Wick, J. D. Lundquist, and M. D. Dettinger, 2008: Meteorological characteristics and overland precipitation impacts of atmospheric rivers affecting the west coast of North America based on eight years of SSM/I satellite observations. *J. Hydrometeor.,* **9,** 22–47, doi:10.1175/2007JHM855.1.

Nijssen, B., R. Schnur, and D. P. Lettenmaier, 2001: Global retrospective estimation of soil moisture using the variable infiltration capacity land surface model, 1980–93. *J. Climate,* **14,** 1790–1808, doi:10.1175/1520-0442(2001)014<1790:GREOSM>2.0.CO;2.

Ralph, F. M., and M. D. Dettinger, 2011: Storms, floods, and the science of atmospheric rivers. *Eos, Trans. Amer. Geophys. Union,* **92,** 265–266, doi:10.1029/2011EO320001.

Shiklomanov, A. I., R. B. Lammers, and C. J. Vörösmarty, 2002: Widespread decline in hydrological monitoring threatens pan-Arctic research. *Eos, Trans. Amer. Geophys. Union,* **83,** 13–17, doi:10.1029/2002EO000007.

Smalley, M., T. L'Ecuyer, M. Lebsock, and J. Haynes, 2014: A comparison of precipitation occurrence from the NCEP stage IV QPE product and the *CloudSat* Cloud Profiling Radar. *J. Hydrometeor.,* **15,** 444–458, doi:10.1175/JHM-D-13-048.1.

Sorooshian, S., K. L. Hsu, X. Gao, H. V. Gupta, B. Imam, and D. Braithwaite, 2000: Evaluation of PERSIANN system satellite-based estimates of tropical rainfall. *Bull. Amer. Meteor. Soc.,* **81,** 2035–2046, doi:10.1175/1520-0477(2000)081<2035:EOPSSE>2.3.CO;2.

Stampoulis, D., E. N. Anagnostou, and E. I. Nikolopoulos, 2013: Assessment of high-resolution satellite-based rainfall estimates over the Mediterranean during heavy precipitation events. *J. Hydrometeor.,* **14,** 1500–1514, doi:10.1175/JHM-D-12-0167.1.

Stokstad, E., 1999: Scarcity of rain, stream gages threatens forecasts. *Science,* **285,** 1199–1200, doi:10.1126/science.285.5431.1199.

Tian, Y., and C. D. Peters-Lidard, 2010: A global map of uncertainties in satellite-based precipitation measurements. *Geophys. Res. Lett.,* **37,** L24407, doi:10.1029/2010GL046008.

——, ——, B. J. Choudhury, and M. Garcia, 2007: Multitemporal analysis of TRMM-based satellite precipitation products for land data assimilation applications. *J. Hydrometeor.,* **8,** 1165–1183, doi:10.1175/2007JHM859.1.

Tobin, K. J., and M. E. Bennett, 2010: Adjusting satellite precipitation data to facilitate hydrologic modeling. *J. Hydrometeor.,* **11,** 966–978, doi:10.1175/2010JHM1206.1.

Turk, F. J., and S. D. Miller, 2005: Toward improved characterization of remotely sensed precipitation regimes with MODIS/AMSR-E blended data techniques. *IEEE Trans. Geosci. Remote Sens.,* **43,** 1059–1069, doi:10.1109/TGRS.2004.841627.

Vila, D., R. Ferraro, and R. Joyce, 2007: Evaluation and improvement of AMSU precipitation retrievals. *J. Geophys. Res.,* **112,** D20119, doi:10.1029/2007JD008617.

Weng, F. Z., L. M. Zhao, R. R. Ferraro, G. Poe, X. F. Li, and N. C. Grody, 2003: Advanced Microwave Sounding Unit cloud and precipitation algorithms. *Radio Sci.,* **38,** 8068, doi:10.1029/2002RS002679.

Westerling, A. L., H. G. Hidalgo, D. R. Cayan, and T. W. Swetnam, 2006: Warming and earlier spring increase western U.S. forest wildfire activity. *Science,* **313,** 940–943, doi:10.1126/science.1128834.

Wilheit, T., C. D. Kummerow, and R. Ferraro, 2003: NASDA rainfall algorithms for AMSR-E. *IEEE Trans. Geosci. Remote Sens.,* **41,** 204–214, doi:10.1109/TGRS.2002.808312.

Wilks, D. S., 2011. *Statistical Methods in the Atmospheric Sciences.* 3rd ed. Academic Press, 676 pp.

Wu, H., R. F. Adler, Y. Hong, Y. Tian, and F. Policelli, 2012: Evaluation of global flood detection using satellite-based rainfall and a hydrologic model. *J. Hydrometeor.,* **13,** 1268–1284, doi:10.1175/JHM-D-11-087.1.

Yilmaz, K. K., T. S. Hogue, K. L. Hsu, S. Sorooshian, H. V. Gupta, and T. Wagener, 2005: Intercomparison of rain gauge, radar, and satellite-based precipitation estimates with emphasis on hydrologic forecasting. *J. Hydrometeor.,* **6,** 497–517, doi:10.1175/JHM431.1.

Zhang, X., E. N. Anagnostou, M. Frediani, S. Solomos, and G. Kallos, 2013: Using NWP simulations in satellite rainfall estimation of heavy precipitation events over mountainous areas. *J. Hydrometeor.,* **14,** 1844–1858, doi:10.1175/JHM-D-12-0174.1.